Article

Influence of water column stratification and mixing patterns on the fate of methane produced in deep sediments of a small eutrophic lake

VACHON, Dominic, *et al*.

Abstract

Methane (CH4), a potent greenhouse gas, is produced in and emitted from lakes at globally significant rates. The drivers controlling the proportion of produced CH4 that will reach the atmosphere, however, are still not well understood. We sampled a small eutrophic lake (Soppensee, Switzerland) in 2016–2017 for CH4 concentrations profiles and emissions, combined with water column hydrodynamics to investigate the fate of CH4 produced in hypolimnetic sediments. Using a mass balance approach for the periods between April and October of both years, net CH4 production rates in hypolimnetic sediments ranged between 11.4 and 17.7 mmol m−2 d−1, of which 66–88% was stored in the hypolimnion, 13–27% was diffused to the epilimnion, and 6–7% left the sediments via ebullition. Combining these results with a process-based model we show that water column turbulent diffusivity (K z) had a major influence on the fate of produced CH4 in the sediments, where higher K z values potentially lead to greater proportion being oxidized and lower K z lead to a greater proportion being stored. During fall when the water column mixes, [...]

Reference

VACHON, Dominic, *et al*. Influence of water column stratification and mixing patterns on the fate of methane produced in deep sediments of a small eutrophic lake. *Limnology and Oceanography*, 2019, vol. 64, no. 5, p. 2114-2128

DOI : 10.1002/lno.11172

LIMNOLOGY and OCEANOGRAPHY

ASLO

Limnol. Oceanogr. 64, 2019, 2114–2128

doi: 10.1002/lno.11172

Influence of water column stratification and mixing patterns on the fate of methane produced in deep sediments of a small eutrophic lake

Dominic Vachon, *[a] Timon Langenegger, Daphne Donis, Daniel F. McGinnis*

Aquatic Physics Group, Department F.-A. Forel for Environmental and Aquatic Sciences (DEFSE), Faculty of Sciences, University of Geneva, Geneva, Switzerland

Abstract

Methane (CH_4), a potent greenhouse gas, is produced in and emitted from lakes at globally significant rates. The drivers controlling the proportion of produced CH_4 that will reach the atmosphere, however, are still not well understood. We sampled a small eutrophic lake (Soppensee, Switzerland) in 2016–2017 for CH_4 concentrations profiles and emissions, combined with water column hydrodynamics to investigate the fate of CH_4 produced in hypolimnetic sediments. Using a mass balance approach for the periods between April and October of both years, net CH_4 production rates in hypolimnetic sediments ranged between 11.4 and 17.7 mmol m^{-2} d^{-1}, of which 66–88% was stored in the hypolimnion, 13–27% was diffused to the epilimnion, and 6–7% left the sediments via ebullition. Combining these results with a process-based model we show that water column turbulent diffusivity (K_z) had a major influence on the fate of produced CH_4 in the sediments, where higher K_z values potentially lead to greater proportion being oxidized and lower K_z lead to a greater proportion being stored. During fall when the water column mixes, we found that a greater proportion of stored CH_4 is emitted if the lake mixes rapidly, whereas a greater proportion will be oxidized if the water column mixes more gradually. This work highlights the central role of lake hydrodynamics in regulating CH_4 dynamics and further suggests the potential for CH_4 production and emissions to be sensitive to climate-driven alterations in lake mixing regimes and stratification.

Lakes are releasing CH_4 to the atmosphere at globally important rates, even though they cover a relatively small area (Bastviken et al. 2011; Kirschke et al. 2013). Although CH_4 can be directly produced in the surface water of lakes (Bogard et al. 2014; Donis et al. 2017), the majority derives from the anoxic sediments as a result of anaerobic degradation of deposited organic carbon (Bastviken et al. 2004*b*; Grasset et al. 2018). To reach the atmosphere, sediment-produced CH_4 must be transported through the water column, where it can be consumed by methanotrophs (Rudd and Hamilton 1978; Utsumi et al. 1998; Kankaala et al. 2006; Bastviken et al. 2008). Sediment-produced CH_4 is transported in the water column by turbulent diffusion (Adams 2005), bubble-mediated transport (McGinnis et al. 2006), plant-mediated transport (Juutinen 2003; Carmichael et al. 2014), or migrating zooplankton (McGinnis et al. 2017; Carey et al. 2018). Although considerable efforts have been invested in quantifying the surface aquatic CH_4 fluxes and the relative contribution of the different emissions pathways (Bastviken et al. 2004*a*; Rinta et al. 2017), the in-lake mechanisms regulating rates of CH_4 production, transport, and oxidation in stratified systems are still poorly understood. Here, we investigate the role of water column hydrodynamics in promoting or restricting the different pathways.

Lake stratification and mixing processes influence the fate of CH_4 produced in the sediments. Although mixing processes in lakes are complex, one cornerstone mechanism for vertical transport of all solutes in stratified waters is the turbulent vertical diffusivity (K_z), which is mainly driven by kinetic energy input (e.g., wind and convection) and water column stability (Imboden and Wüest 1995; Read et al. 2012). Turbulent vertical diffusivity partly regulates the magnitude of vertical fluxes across the thermocline (Kreling et al. 2014). Strong water column stratification therefore limits vertical gas exchange between the hypolimnion and epilimnion resulting in increasing bottom water CH_4 storage (Juutinen et al. 2009; Kankaala et al. 2013; Rinta et al. 2017). High oxidation rates are often observed near the thermocline of stratified lakes, where both CH_4 and O_2 concentrations overlap (Sundh et al. 2005;

*Correspondence: domvachon@gmail.com; daniel.mcginnis@unige.ch

Additional Supporting Information may be found in the online version of this article.

[a]Present Address: Department of Ecology and Environmental Science, Umeå University, Umeå, Sweden

Oswald et al. 2016), although microaerobic CH_4 oxidation can also occur just below the chemocline in anoxic waters (Blees et al. 2014). Furthermore, high K_z values were associated with high rates of CH_4 oxidation in Lake Mendota (Fallon et al. 1980), whereas low K_z values were associated with low oxidation rates in Lake 227 (Rudd and Hamilton 1978). Taken together these studies highlight the role of K_z on CH_4 oxidation and storage in stratified lakes.

The transport through the water column via rising bubbles (i.e., ebullition) account for about half of the total CH_4 emission in lakes (Bastviken et al. 2004*a*). Ebullition allows a fraction of methane to bypass the oxidation barrier and therefore efficiently conveys sediment-produced CH_4 to the atmosphere (McGinnis et al. 2006). When net gas production (mainly CH_4 but also CO_2, N_2O, and N_2) rates occur faster than the diffusive flux out from the sediments, the dissolved CH_4 in porewater can reach oversaturation (i.e., total gas pressure exceeds absolute pressure at depth) and CH_4 ebullition will occur (Schmid et al. 2017). Ebullition is more frequent in shallow sediments (Bastviken et al. 2004*a*) due to the role of hydrostatic pressure in regulating bubble formation. In deeper sediments, the critical CH_4 concentration at which bubbles form is higher due to increased solubility with lower temperatures and higher pressures. For these reasons, only systems with intense sediment CH_4 production are able to form bubbles from deep sediments (West et al. 2016) or in meromictic lakes where bubble formation can benefit from the important total gas pressure accumulated in the trapped bottom waters (Horn et al. 2017).

In fall when deeper vertical mixing occurs, CH_4-rich bottom waters are rapidly mixed with surface oxygenated waters. This results in enhanced CH_4 oxidation rates (Rudd and Hamilton 1978; Kankaala et al. 2006) but also to higher diffusive fluxes to the atmosphere. Atmospheric CH_4 emission during lake turnover usually corresponds only to about 15% to 45% of the CH_4 stored in the hypolimnion (Rudd and Hamilton 1978; Kankaala et al. 2006; Schubert et al. 2012; Encinas Fernández et al. 2014). However, the vertical mixing process in fall is not always complete, where accumulated CH_4 during summer can remain trapped in the bottom waters over winter. The accumulation of solutes in the deep layers during summer increases the bottom water stability and can prevent the lake from complete mixing (i.e., biogenic meromixis; Boehrer et al. 2017; Schultze et al. 2017). The ultimate fate of this longer term CH_4 storage induced by incomplete vertical mixing, and its potential impact on lake CH_4 dynamics has rarely been reported (*see* Itoh et al. 2015).

Here, we investigate the interaction among CH_4 transport pathways, fate, and specific physical environmental characteristics such as water column stability and length of stratification period. We hypothesize that (1) higher water column stability during summer stratification results in reduced upward turbulent CH_4 flux and higher CH_4 storage (Fig.1) and that (2) increasingly isolated hypolimnion due to longer stratification periods or incomplete turnover promotes higher CH_4 concentrations, CH_4 production, and CH_4 ebullition from deep sediments (Fig. 1). To test these hypotheses, we measured hypolimnetic CH_4 dynamics and deep sediments ebullition from a small eutrophic lake (Soppensee, Switzerland) over approximately two full years. Using mass balance approaches, we estimate net CH_4 production in the hypolimnion and its fate during the stratified and mixing period. We then use a simple process-based model to further investigate the potential role of water column stratification strength for CH_4 fate. We concluded that water column physical structure and hydrodynamics affect the fate of CH_4 produced in the deep sediments by reallocating the oxidation and emissions pathways. Moreover, we show that an incomplete mixing in winter 2016/2017 had critical implications for the following summer CH_4 dynamics and during the following year complete turnover event.

Methods

Study site and sampling frequency

The study was conducted in the small eutrophic lake Soppensee (47.09°N, 8.08°E) situated in the Canton of Lucerne, Switzerland (lake area: 23 ha, maximum depth: 26 m, mean depth: 12.2 m). Average total phosphorus integrated over the whole water column was about 70 μg P L^{-1} in 2016–2017. The lake was sampled on a ~ monthly basis (more frequently in summer but less in winter) from April 2016 to January 2018 (discussed below). In addition to manual sampling, moored instruments were deployed for continuous measurements of temperature and oxygen. Inverted funnels (3) were deployed for gas ebullitive fluxes from deep sediments. During summer, sediment cores were taken to estimate the porewater CH_4 concentration and potential CH_4 production (August–September 2016 and July–September in 2017). A bathymetric map of Soppensee with the location of the moored instruments and gas funnels is shown in Supporting Information Fig. S1.

Water temperature and dissolved oxygen

In the deepest point of the lake (~ 26 m; Supporting Information Fig. S1), a string of temperature loggers (Vemco Minilog-II-T; temperature accuracy ± 0.1°C, resolution 0.01°C) was moored from 26 April 2016 to January 2018, measuring water temperature every minute at several depths (2, 5, 8, 10.8, 13.5, 16, 18.5, 23, and 26 m). In 2017, seven additional loggers were added to the mooring (1, 4, 6.5, 12.1, 14.7, 19.8, and 21 m). A dissolved O_2 probe (miniDOT, Precision Measurements Engineering) was installed at 1 m depth and logged temperature, dissolved O_2 concentration (mg O_2 L^{-1}), and saturation (%) every minute.

In addition to continuous measurements, manual CTD (conductivity, temperature, depth and dissolved oxygen) profiles were performed every 3-weeks to 1-month intervals using a multiparameter sonde (Yellow Spring Instrument EXO2, after May 2017 a Seabird pumped CTD profiler, SBE19). Water column stability was calculated as $N^2 = -\frac{g}{\rho}\frac{\partial \rho}{\partial z}$ (s^{-2}), where g is the gravitational acceleration (m s^{-2}), z is the depth (m), and ρ is the water density (kg m^{-3}). Water density was calculated using

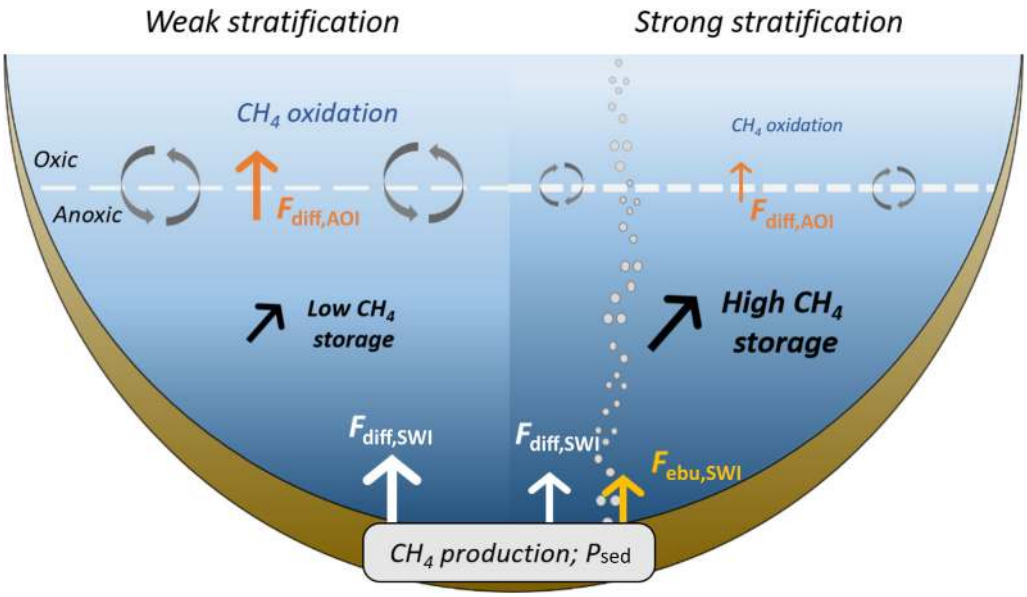

Fig. 1. Conceptual scheme of CH_4 dynamics under weak (left) and strong (right) water column stratification in a small eutrophic lake. Methane is produced in sediments (net CH_4 production; P_{sed}; gray box) and can either leave by diffusion at the sediment–water interface ($F_{diff,SWI}$; white arrows) or by ebullition ($F_{ebu,SWI}$; yellow arrow). Once in the anoxic bottom waters, CH_4 will accumulate (storage; black arrow) and diffuse through the AOI ($F_{diff,AOI}$; orange arrows) where it is potentially oxidized.

temperature (T) and specific conductivity at 20°C (κ_{20}) from the CTD profiles (Imboden and Wüest 1995, eqs. 29 and 35). The O_2 profiles from May to October were used to determine the anoxic–oxic interface (AOI) for the mass balance purpose (here determined to be at 8 m), which corresponds to the depth at which dissolved O_2 is below 1 mg L^{-1}.

Vertical turbulent diffusivities (K_z) below 5 m were estimated for each sampling date during the stratified periods using the heat budget method (Jassby and Powell 1975). The continuous temperature measurements were used to calculate the temporal rates of temperature change. This method assumes that turbulent transport of heat at depth z is a function of the rate of change of heat content below that depth. Rates of heat transfer were calculated as the slope of temperature change over time measured between 7 d before and after each sampling date. These temperature slopes were vertically linearly interpolated at each meter depth and CTD profiles were used to calculate the vertical temperature gradient with depth (Wüest et al. 2000). We assumed that solar radiation had minimal direct effect on the temperature change below 5 m as the lake was turbid, with the averaged measured Secchi depth of about 2 m. As a result, a K_z profile from 5 m to bottom was resolved for each sampling date, which corresponds to the integrated K_z over about 14 d (7 d before and after the sampling date).

Methane concentration and stable isotope (δ^{13}C-CH_4)

Dissolved CH_4 and stable C isotope values (δ^{13}C-CH_4) in the water column were measured using a 1-liter bottle headspace method as described in Donis et al. (2017). Briefly, lake water was sampled at defined depth using a 5-liter Niskin water sampler. The vertical sampling resolution was variable between the sampling dates, but samples were taken usually every 1–3 m down to 10 m and then every 5 m down to the bottom. Water from the Niskin bottle was gently poured into a 1-liter glass bottle, letting overflow to replace 1-liter bottle volume several times. A volume of 400 mL of water was carefully removed and replaced with ambient air without creating turbulence. The bottle was capped and shaken vigorously for at least 2 min. The headspace was transferred into a gas-tight atmospheric sampling bag (Supel™ Inert Multi-Layer Foil) for further gas analysis on a Cavity Ring-Down Spectrometer (Picarro G2201-i). In case of high CH_4 concentration (e.g., samples below 10 m in Soppensee), an additional dilution was applied before the analysis by subsampling the bag and diluting into a 50 mL glass gas-tight syringe (SGE Analytical Science) filled with synthetic air (Carbagas: 80% N_2, 20% O_2; ± 1%). In these cases, the gas was subsampled two or three times and the average was taken. The average coefficient of variation (C.V.) for all these diluted replicates was 5% (n = 67). Lake water dissolved CH_4 concentration and δ^{13}C-CH_4 was back calculated by applying a mass balance in the bottle, with information about air CH_4 concentration, water temperature, and atmospheric pressure. A second sample was occasionally taken for a given depth to test for replicability of the method. The average C.V. for all the replicates was 9.7% (n = 8).

CH_4 ebullitive fluxes

We measured ebullition fluxes from sediments below 8 m using bubble traps made of inverted funnels with bubble collectors (DelSontro et al. 2010). In May 2016, two bubble traps (opening of 0.79 m^2) were deployed about 4 m below the

surface water over sediments of 10 and 21 m depths. Another bubble trap (also 0.79 m^2) was installed in June 2017 over 15 m deep sediments to provide a better spatial coverage, also moored at about 4 m below surface (*see* Supporting Information Fig. S1 for Soppensee map with bubble traps locations). Bubble traps were moored with an inverted-V configuration to avoid disturbing the sediments below them. At each sampling date, the traps were gently brought to the surface and the gas volume was sampled using a 60-mL plastic syringe with a needle through the gas collector septum. Total gas volume was converted to moles of gas according to the Ideal Gas Law using in situ temperature and atmospheric pressure at the day of sampling. Total gas flux (mmol m^{-2} d^{-1}) received by the funnel (sitting at 4 m depth) was calculated accounting for funnel area, gas volume sampled, and deployment duration. When bubbles rise from the sediments to the funnel, the different gases in the bubble exchange with the water column. To convert to total gas (and CH_4) fluxes at the sediment water interface (SWI), a correction for gas exchange of the rising bubbles was made using a single bubble simulation model (McGinnis et al. 2006). The bubble model simulations estimated that about 30% of CH_4 in the rising bubble was dissolved back in the hypolimnion (below 8 m). Further information for these steps is provided in the Supporting Information Section S1.

Methane ebullition fluxes were extrapolated to the whole hypolimnetic area (i.e., sediment area below 8 m) by allocating the three funnel-derived results to three different bathymetric zones. We multiplied the rates from the 10-m funnel with the sediment area between 8 and 14 m, rates from the 15-m funnel with the area between 15 and 21 m, and the 21-m funnel rates with the area between 21 and 26 m. The sum of ebullition from these areas was then divided by the sediment area below 8 m to get the integrated CH_4 ebullition below 8 m (mmol m^{-2} d^{-1}). As we did not install a funnel at 15 m in 2016, ebullition rates from 15 m depth in 2016 were extrapolated using a linear relationship linking ebullition rates at 10 and 15 m using the 2017 data ($n = 10$, $r^2 = 0.30$).

Diffusive CH_4 fluxes at AOI

Diffusive flux at the AOI ($F_{diff,AOI}$; mmol m^{-2} d^{-1}) was estimated following Fick's First Law:

$$F_{\mathrm{diff,AOI}} = K_{z,\mathrm{AOI}} \frac{\partial \mathrm{CH_4}}{\partial z} \quad (1)$$

The CH_4 concentration gradient ($\frac{\partial CH_4}{\partial z}$) crossing the AOI was determined from CH_4 measurements between 7 and 10 m. $K_{z,AOI}$ was determined from derived K_z values from the heat budget method and log-averaged between 7 and 10 m to match the associated CH_4 gradient thickness.

Diffusive CH_4 flux measurements at the air–water interface

Surface diffusive CH_4 fluxes with the atmosphere were measured using a floating chamber connected in a closed loop to a portable greenhouse gas analyzer (Los Gatos Research) as described in McGinnis et al. (2015). At each sampling occasion, a series of three to six chamber deployments were performed from the boat at the center of the lake during the day (between 9:00 and 16:00 h). Each deployment lasted about 6 min, and diffusive flux was calculated as the slope of the linear CH_4 increase (McGinnis et al. 2015).

Hypolimnetic CH_4 mass balance

We used a CH_4 mass balance approach during the stable stratified period (May to October) of both studied years. The daily change in CH_4 storage below 8 m ($\frac{\Delta C_{CH_4}}{\Delta t} V_{hypo}$; mmol d^{-1}) is described as:

$$\frac{\Delta C_{\mathrm{CH_4}}}{\Delta t} V_{\mathrm{hypo}} = \alpha F_{\mathrm{ebu,SWI}} A_{\mathrm{sed}} + F_{\mathrm{diff,SWI}} A_{\mathrm{sed}} - F_{\mathrm{diff,AOI}} A_{\mathrm{AOI}} \quad (2)$$

where $F_{ebu,SWI}$ (mmol m^{-2} d^{-1}) is the ebullition of CH_4 leaving the sediments, α is the dissolution factor of CH_4 from bubbles into the hypolimnetic water (0.3; determined from the bubble simulation), $F_{diff,SWI}$ (mmol m^{-2} d^{-1}) is the diffusion of CH_4 across the SWI, $F_{diff,AOI}$ (mmol m^{-2} d^{-1}) is the diffusion from hypolimnion to the epilimnion across the AOI, A_{sed} (m^2) is the sediment area, and A_{AOI} (m^2) is the area at the AOI (8 m). As the hypolimnion was anoxic during the integration period, we assumed that CH_4 oxidation was insignificant compared to the other fluxes (Schmid et al. 2017). However, we acknowledge that anaerobic CH_4 oxidation (Reed et al. 2017) and microaerobic CH_4 oxidation (Blees et al. 2014) might however have occurred (*see* Discussion section for implication on the results). Change in CH_4 storage below 8 m was calculated as the linear increase of the volume-weighted average CH_4 concentration of the sampling dates between May and October each year ($n = 7$ in 2016 and $n = 6$ in 2017). For each sampling date, the volume-weighted average CH_4 concentration was estimated from the vertical linear interpolation of measured CH_4 concentrations combined with volume of each depth strata below 8 m. $F_{ebu,SWI}$ was estimated as the temporally averaged ebullition below 8 m over the integrated period of the mass balance each year (as the cumulative ebullition divided by the number of days). $F_{diff,AOI}$ is the average diffusive flux at the AOI of the same sampling date included in the mass balance period. By rearranging Eq. 2, we can derive the temporally integrated and spatially integrated diffusion at the SWI ($F_{diff,SWI}$) as:

$$F_{\mathrm{diff,SWI}} = \left[\frac{\Delta C_{\mathrm{CH_4}}}{\Delta t} V_{\mathrm{hypo}} - \alpha F_{\mathrm{ebu,SWI}} A_{\mathrm{sed}} + F_{\mathrm{diff,AOI}} A_{\mathrm{AOI}} \right] / A_{\mathrm{sed}} \quad (3)$$

Similarly, by assuming the rate of net CH_4 production in the sediment is equal to the CH_4 transported out via methane flux and ebullition, then the temporally integrated and spatially integrated net CH_4 production (P_{sed}) can be defined as:

$$P_{\mathrm{sed}} = F_{\mathrm{ebu,SWI}} + F_{\mathrm{diff,SWI}} \quad (4)$$

As the mass balance equations consist in sources (additions) and sinks (subtractions), we assessed the general uncertainties of P_{sed} and $F_{diff,SWI}$ by applying the rule of error propagation as:

$$\sigma Q = \sqrt{(\sigma A)^2 + (\sigma B)^2 + (\sigma C)^2 + \dots} \quad (5)$$

where σQ is the uncertainty around a quantity Q (here P_{sed} and $F_{diff,SWI}$) and σA, σB, and σC are the uncertainties of each component of the mass balance equation ($F_{ebu,\ SWI}$, $\frac{\Delta C_{CH_4}}{\Delta t}$, $F_{diff,\ AOI}$ in Eq. 3 and $F_{ebu,\ SWI}$, $F_{diff,\ SWI}$ for Eq. 4). Here, we use the term uncertainty as a general assessment of error due to methodology and/or intermittency of the processes. Uncertainty in $\frac{\Delta C_{CH_4}}{\Delta t}$ was determined as the standard error of the linear slope (LINEST function in Microsoft Excel), and uncertainty in $F_{diff,\ AOI}$ was determined as the standard deviation of the estimated fluxes at each sampling date during the integrated mass balance period. For $F_{ebu,SWI}$, the uncertainty can be due to the methods (e.g., bubble model correction and interpolation of the missing ebullition measurement at 15 m in 2016) and to the spatial variability of ebullition. Previous study by Wik et al. (2016) suggested that for two to three sampling locations (like in our case), the risk of overestimating or underestimating ebullition fluxes is between 25% and 50%, with more risk of underestimating. As we believe that the uncertainty is mainly due to spatial variability, we applied a conservative 50% uncertainty around the average $F_{ebu,SWI}$ used in the mass balance. As $F_{ebu,SWI}$ contribution to the mass balance was relatively small compared to the other components, the ebullition uncertainty did not significantly influence the final production and diffusion estimates (*see* Discussion section for further details).

Hypolimnetic CH_4 dynamics model

The observed dynamics among CH_4 storage, net production, diffusion fluxes at the SWI and AOI, and CH_4 ebullition at SWI were reproduced with a simple process-based model (Supporting Information Fig. S2). The model main equation was directly derived from the mass balance (Eq. 2) to predict hypolimnetic CH_4 ($[CH_4]_{hypo,t}$) concentration and was solved numerically with the Euler method with a daily time step (Δt):

$$[CH_4]_{hypo,t} = [CH_4]_{hypo,t-1} + \left[F_{diff,SWI}\frac{A}{V} - F_{diff,AOI}\frac{A}{V} + \alpha F_{ebu,SWI}\frac{A}{V}\right]\Delta t \quad (6)$$

where $F_{diff,SWI}$ is the diffusion flux at the sediment–water interface, $F_{diff,AOI}$ is the flux across the AOI and was a function of $K_{z,eff} \times [CH_4]_{hypo,t}$, and the ebullition $F_{ebu,SWI} = P_{sed} - F_{diff,SWI}$. However, for ebullition to occur, P_{sed} has to be greater than the maximum $F_{diff,SWI}$, determined as $k_{sed} \times ([CH_4]_{pw,crit} - [CH_4]_{hypo,t})$. If P_{sed} is smaller than the maximum $F_{diff,SWI}$, no ebullition occurs and $P_{sed} = F_{diff,SWI}$ (Supporting Information Fig. S2). $[CH_4]_{pw,crit}$ is the critical CH_4 concentration in the porewater of sediment over which bubbles can form (i.e., local pressure > atmospheric + hydrostatic pressures assuming N_2 as the only other gas contributing to total gas pressure). If we assume that N_2 partial pressure (pN_2) in the porewater is equivalent to atmospheric pN_2, i.e., 79%, then the CH_4 partial pressure (pCH_4) required to form bubbles in the porewater is estimated as $pCH_4 = local_{pressure} - 0.79 \times atm_{pressure}$. Local pressure ($local_{pressure}$) was determined as $atm_{pressure} + \frac{\rho \times z \times g}{101325}$, where $atm_{pressure}$ is in atm, ρ is the density of water (~ 1000 kg m^{-3}), z is the depth of the sediments (m), and g is the gravitational acceleration (9.81 m s^{-2}). This critical pCH_4 was converted to $[CH_4]_{crit}$ using Henry's Law (Sander 1999) and averaged 4870 μmol L^{-1} for Soppensee hypolimnetic sediments (mean depth of 15.5 m at water temperature of 5.6°C and local atmospheric pressure of 0.94 atm). Note also that $[CH_4]_{crit}$ is assumed to be constant over time, however, processes like porewater stripping of other dissolved gases (i.e., N_2) may slightly influence this value (Chanton et al. 1989; Langenegger et al. 2019). k_{sed} is the gas transfer velocity (m d^{-1}) at the SWI and $K_{z,eff}$ is the effective turbulent diffusivity over 1 m at the AOI (m^2 d^{-1}). To test the model behavior, we parameterize k_{sed} to fit the average observed diffusive flux at SWI determined by the mass balance $F_{diff,SWI}$, and $K_{z,eff}$ to fit the average observed $F_{diff,AOI}$ (*see* Supporting Information Section S2 for further details on model and Table S1 for model calibration parameters).

Estimating CH_4 emissions during lake turnover

The proportion of CH_4 emission during the lake turnover was estimated as the average CH_4 flux at the air–water interface ($F_{CH_4,AWI}$) divided by the whole water-column CH_4 mass loss. Whole water-column CH_4 mass loss was estimated from the linear decrease in whole water-column CH_4 mass (mmol m^{-2}) measured during the lake turnover period, i.e., from 17 November 2016 to 10 March 2017 for the first year and from 02 November 2017 to 23 January 2018 for the second year. The whole water-column CH_4 mass was estimated on each sampling occasion from the vertical linear interpolation of measured CH_4 concentration, multiplied by the volume of each meter strata and divided by the lake surface area.

Surface CH_4 diffusive emissions during the turnover periods was estimated using Fick's First Law of diffusion as:

$$F_{CH_4,AWI} = k_{CH_4}\left([CH_4]_{sw} - [CH_4]_{eq}\right) \quad (7)$$

where k_{CH_4} is the daily gas transfer velocity (m d^{-1}), $[CH_4]_{sw}$ is the daily surface water CH_4 concentration interpolated linearly from the monthly sampling, and $[CH_4]_{eq}$ is the CH_4 concentration in equilibrium with the atmosphere. Gas transfer velocity (k_{CH_4}) was estimated from standardized gas transfer velocity (k_{600}) derived from a wind-based model developed during positive buoyancy flux (MacIntyre et al. 2010) using daily averaged wind speed measured from a meteorological tower situated about 12 km north of the lake (Egolzwil station,

Federal Office of Meteorology and Climatology MeteoSwiss). A portable weather station (Kestrel 3000) was deployed occasionally in the center of the lake (two deployments of about 2–3 h) on October 2016 and August 2017. When comparing both wind speed measurements corrected to 10 m height (Crusius and Wanninkhof 2003), systematically lower U_{10} was recorded on the lake than at the Egolzwil station due to the wind shelter effect by the surrounding trees and hills, whereas the inland meteorological tower is situated in an open field. An empirical correction was therefore used to infer the Egolzwil measured U_{10} for the lake situation (Supporting Information Fig. S3; $U_{10Sopp} = 0.515 \times U_{10tower}$, $r^2 = 0.95$, $n = 55$). The relationship covered a range of recorded U_{10} between 0.2 and 7.4 m s^{-1}. Then, k_{600} was converted to k_{CH_4} (Jähne et al. 1987) using CH_4 Schmidt number estimated from surface water temperature (Wanninkhof 1992) and using n exponent of −2/3 for smooth surfaces. $[CH_4]_{eq}$ is the water concentration in equilibrium with the atmosphere (assuming constant atmospheric pCH_4 of 2 μatm and using Henry's Law).

Results

Stratification and mixing patterns

In both 2016 and 2017, the lake water column was strongly thermally stratified from May to October (Fig. 2a), with the thermocline situated between 5 and 7 m depth. Water temperature in summer normally reached about 24–26°C in the surface layer and remained at around 4–5°C in the bottom water throughout the year. During the summer, specific conductivity (κ_{20}; μS cm^{-1}) decreased in the surface waters, reaching values around 250 μS cm^{-1}, and increased in the hypolimnion with values reaching ~ 400 μS cm^{-1} (Fig. 2b). During the first winter (Dec 2016–March 2017), ice formed for approximately 50 d (from beginning of January until end of February 2017). The buildup of solutes as indicated from the specific conductivity in the hypolimnion increased the bottom water density. Combined with the development of the ice cover, the higher density of the hypolimnetic water prevented complete turnover during the first winter. During winter of the second year (January 2018), the water column was mixed completely and more rapidly (Fig. 2a,b).

We used monthly profiles of temperature and specific conductivity to calculate the water column stability (N^2). Continuous measurements of water column temperature from the moored temperature loggers and profiles were used to estimate the basin-scale vertical turbulent diffusivity profiles (K_z). Average N^2 between 6 and 10 m (log-average) increased from low values in early spring (from about 10^{-4} s^{-2}) to up to maximum values in August and September of both years (around 10^{-3} s^{-2}; Supporting Information Fig. S4a). In October, N^2 between 6 and 10 m decreased sharply to low values around November (down to around 10^{-4} s^{-2}). From April to October, K_z values between 6 and 10 m (log-average) were comparable between 2016 (4.2×10^{-7}–2.1×10^{-6} m^2 s^{-1}) and 2017 (3.5×10^{-7}–3.8×10^{-6} m^2 s^{-1}), with minimum diffusivities occurring in October and late August for 2016 and 2017, respectively (Supporting Information Fig. S4b). Average K_z values just below (11–15 m) were slightly lower in 2016 (8.5×10^{-7}–4.9×10^{-6} m^2 s^{-1}) compared to 2017 (1.3×10^{-6}–1.0×10^{-5} m^2 s^{-1}; Supporting Information Figs. S4b, S5). Taking both years together, average N^2 and K_z values (between 6 and 10 m) showed a strong negative relationship (Supporting Information Fig. S6).

Dissolved oxygen dynamics

The stratified water column during summer of both years led to an extended period of hypolimnetic anoxia (here defined as dissolved $O_2 < 1$ mg L^{-1}) between May to October (Fig. 2c). The transition between anoxic and oxic waters (defined as the AOI) varied slightly between 6 and 9 m during the summer stratification and also corresponded to the upper limit of the hypolimnion for both years (here assumed to 8 m). Although temporal resolution of sampling in winter was coarse, we did not measure O_2 above 1 mg L^{-1} below 19 m during winter 2016–2017, while in January 2018, bottom O_2 concentrations were above 1 mg L^{-1} down to 25 m after turnover (Fig. 2c). In the surface waters, O_2 saturation was highly variable, with periods of O_2 oversaturation (> 100%) down to 5 m depth (Fig. 2c,d). The highest O_2 saturation values were measured between August and September 2016, with values reaching over 200% saturation (Fig. 2c,d). In 2017, extensive oversaturation values (up to about 175%) were observed between early May and mid-July (Fig. 2d). Between November and March, surface O_2 saturation was usually below 100% and decreased drastically to 0% for ~ 10 d in January 2018 during the complete lake overturn (Fig. 2d).

Lake CH_4 concentration, storage, and vertical fluxes

Figure 3 shows the vertical profiles of dissolved CH_4 concentrations and their C stable isotopes (δ^{13}C-CH_4). Dissolved CH_4 concentration reached the highest values near the bottom (25 m), starting from 30 μmol L^{-1} (April 2016), and due to incomplete turnover, starting at ~ 300 μmol L^{-1} in April 2017. Maximum concentrations of ~ 1300 μmol L^{-1} were observed in November during both 2016 and 2017 (Figs. 3–4a). Dissolved CH_4 was significantly lower and relatively constant at the lake surface, ranging between 0.5 and 1.5 μmol L^{-1} between April and October of both years and increasing during fall convective mixing to values up to ~ 7 μmol L^{-1} in November 2016 and up to 54.5 μmol L^{-1} in December 2017. During the well-stratified seasons, CH_4 concentrations were the lowest near the thermocline just above the AOI (between 5 and 8 m depth; Fig. 3a,c) with values around 0.3–0.5 μmol L^{-1}; however, winter surface CH_4 concentrations were even lower around 0.01 μmol L^{-1} (Fig. 3b,d). During the well-stratified periods, values of δ^{13}C-CH_4 were around −66‰ below 10 m, associated with the highest CH_4 concentrations, while ranging between −56‰ and −35‰ in the surface waters (Fig. 3a,c). δ^{13}C-CH_4 values were the highest (around −20‰) around the thermocline (5–7 m) just

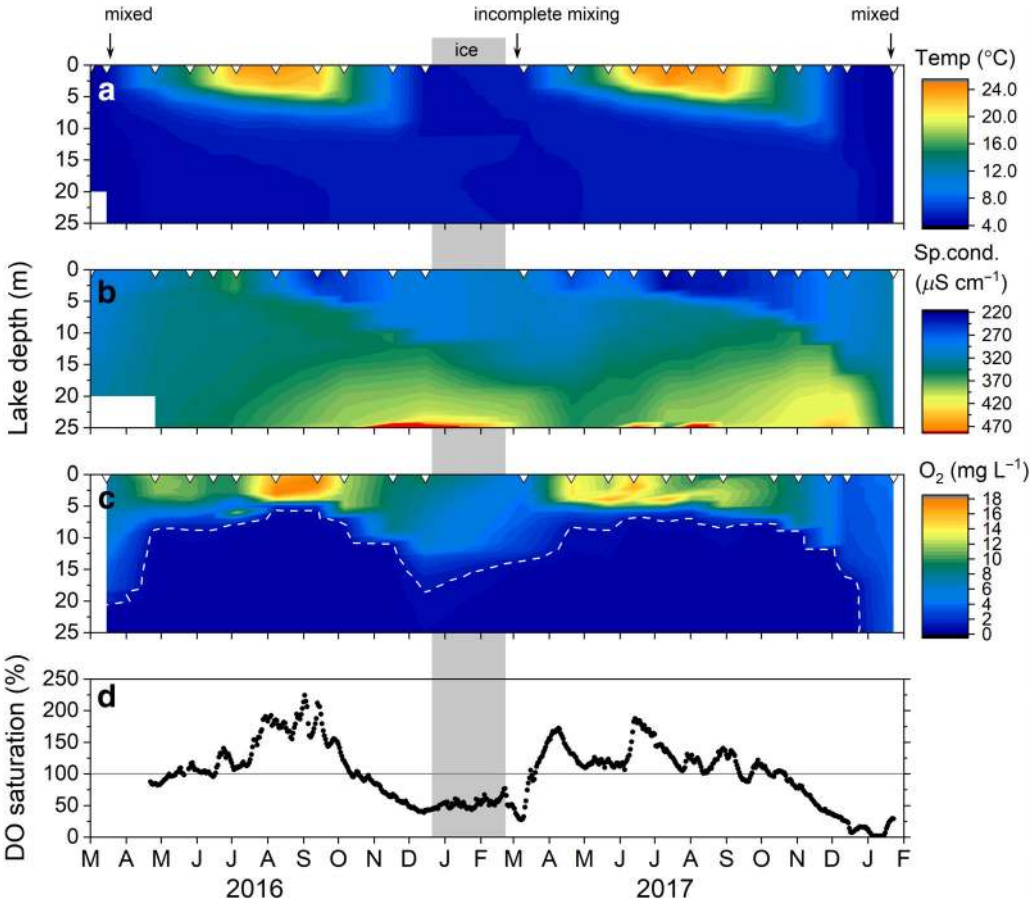

Fig. 2. Water column time series of (**a**) water temperature, (**b**) specific conductivity at 20°C, and (**c**) dissolved oxygen saturation. The white dashed line in panel (**c**) represents the isoline of 1 mg O_2 L^{-1} (anoxia). The sampling dates are identified by the small white triangles. Panel (**d**) shows the time series of surface dissolved O_2 saturation (%) logged every minute at 1 m depth. Light gray area shows the ice cover extent during winter 2016–2017.

above the AOI and are associated with the lowest CH_4 concentrations (Fig. 3a,c). During fall mixing and winter, δ^{13}C-CH_4 values were higher at the surface (between −40‰ and −30‰), whereas the bottom waters δ^{13}C-CH_4 values were low at around −65‰ (Fig. 3b,d).

Volume-weighted average CH_4 concentrations below 8 m increased linearly with a higher rate observed in 2017 (1.6 μmol L^{-1} d^{-1}) than in 2016 (1.2 μmol L^{-1} d^{-1}; Fig. 4b). Due to the incomplete mixing event, the entire water column CH_4 storage was about 10 times higher in April 2017 (697 mmol m^{-2}) than during the same time of the previous year (72 mmol m^{-2}). Water column storage also reached the highest values in November 2017 (2402 mmol m^{-2}) compared to the same period in 2016 (1320 mmol m^{-2}). During fall, whole-lake CH_4 storage decreased at a rate of −7.8 mmol m^{-2} d^{-1} in 2016/2017 (incomplete mixing). In 2017/2018, the whole-lake storage decreased almost 4 times faster (−28.8 mmol m^{-2} d^{-1}; Fig. 4b).

Between May and October 2016, $F_{diff,AOI}$ varied between 0.4 and 2.6 mmol m^{-2} d^{-1}, averaging 1.5 ± 0.9 mmol m^{-2} d^{-1} (n = 6). Between May and October 2017, $F_{diff,AOI}$ varied between 1.9 and 6.7 mmol m^{-2} d^{-1}, averaging 4.7 ± 1.8 mmol m^{-2} d^{-1} (n = 6). During the well-stratified period (May to October) surface diffusive CH_4 fluxes to the atmosphere measured with floating chambers were on average 1.4 ± 1.0 mmol m^{-2} d^{-1} (± 1 SD; n = 69) and 1.8 ± 0.9 mmol m^{-2} d^{-1} (± 1 SD; n = 39) for 2016 and 2017, respectively. In November and December 2016, we measured surface diffusive CH_4 fluxes of 3.1 ± 0.3 mmol m^{-2} d^{-1} (± 1 SD; n = 3) and 0.6 ± 0.2 mmol m^{-2} d^{-1} (± 1 SD; n = 7), respectively. In November and December 2017, surface diffusive CH_4 fluxes were on average 2.1 ± 0.9 mmol m^{-2} d^{-1} (± 1 SD; n = 13) and 141.3 ± 18.4 mmol m^{-2} d^{-1} (± 1 SD; n = 6), respectively.

Ebullitive CH_4 fluxes

Ebullition flux measured with bubble traps varied significantly both temporally (interannual and intraannual) and spatially between the different locations (Supporting Information Fig. S7a,b). Total gas fluxes were converted to CH_4 bubble gas leaving the sediment (hereafter referred to as ebullition). Ebullition at 10 m depth usually showed the highest rates, often two times higher than ebullition at 21 m depth (Supporting Information Fig. S7b). The lowest ebullition rates were measured at the 15-m funnel site (Supporting Information Fig. S7a,b). Spatially averaged CH_4 ebullition rates were estimated for sediments below 8 m and are shown on Fig. 4c (*see* Supporting Information

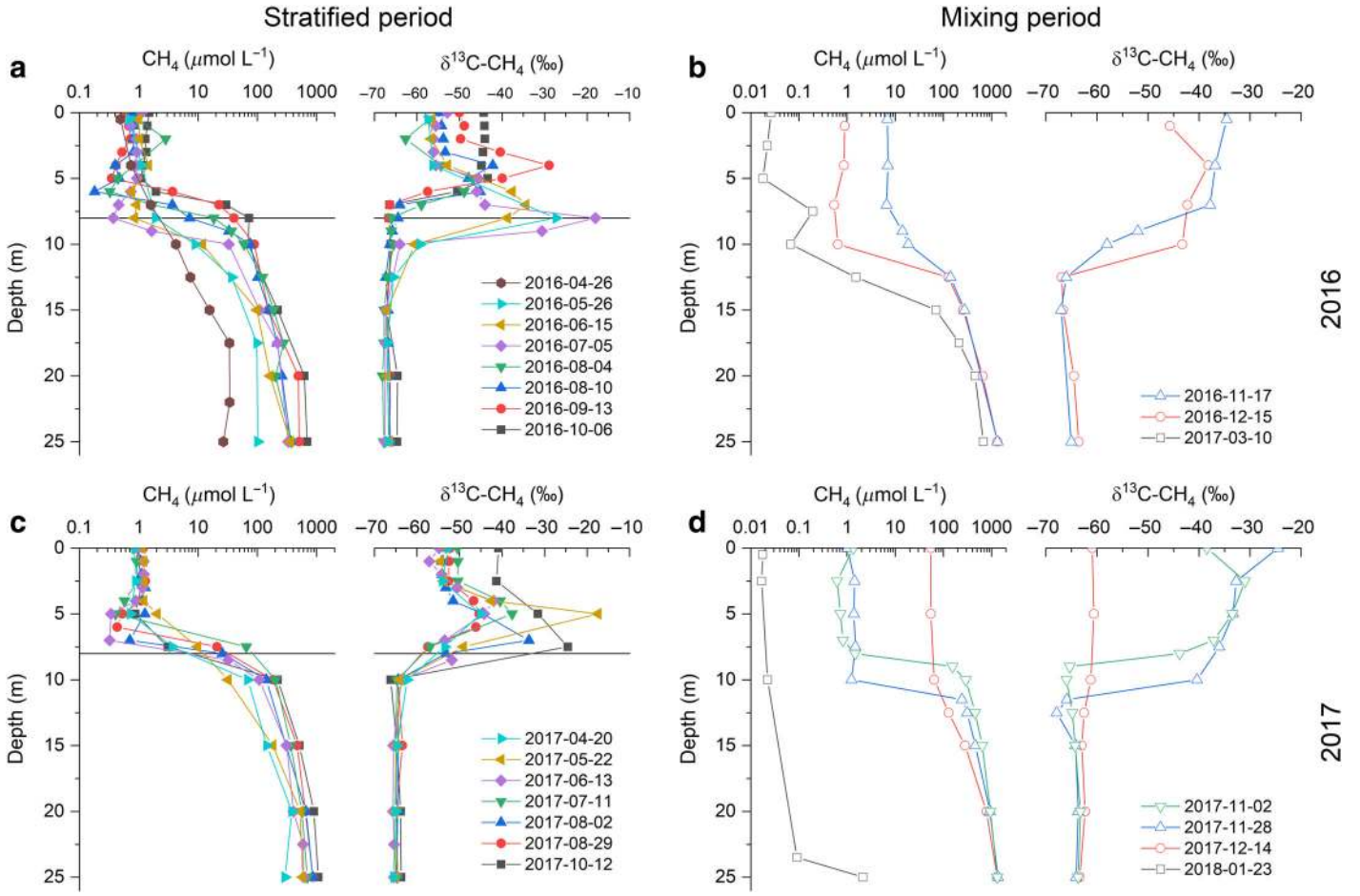

Fig. 3. Water column measurements of CH_4 concentration and its C stable isotopes signature in 2016 (**a**, **b**) and 2017 (**c**, **d**), for the well-stratified periods (late-April to early-October; **a**, **c**) and the mixing periods (November to March; **b**, **d**). Horizontal lines in (**a**) and (**c**) represent the AOI at 8 m. Note that no isotopes measurements were available for the 26 April 2016, 10 March 2017, and 23 January 2018 profiles.

Fig. S7b and Methods section for details). In 2016, ebullition began in early June and gradually increased to up to about 2.0 mmol m^{-2} d^{-1} toward the end of the year. In winter 2016–2017, ebullition slowed down to ~ 0.5 mmol m^{-2} d^{-1}. Between June and November 2017, ebullition below 8 m varied between 1.4 and 2.7 mmol CH_4 m^{-2} d^{-1} (Fig. 4c). In December 2017, ebullition decreased to about 1 mmol m^{-2} d^{-1} and completely stopped after turnover with no ebullition observed at any funnel from 23 January to 10 April 2018.

CH_4 mass balance and system analysis during the stratified periods

We performed a mass balance to derive spatially integrated and temporally integrated rates of net CH_4 production in sediments and CH_4 diffusion at the SWI during the stratified season. The mass balance revealed that net CH_4 production in the hypolimnetic sediments (below 8 m) in 2017 was ~ 1.6 times higher than the net production in 2016 (Table 1). Over the integrated period of the mass balance, ebullition flux in 2017 was almost two times higher than in 2016, and the proportion of production that left via ebullition was similar (8% and 11%), although slightly higher in 2017 (Table 1). The sediment diffusive flux at the SWI accounts for ~ 90% of the CH_4 leaving the sediment (Table 1), and the majority of the CH_4 produced in the sediments was stored in the hypolimnion (81% in 2016 and 66% in 2017), including the 30% redissolution of bubble CH_4.

To evaluate the role of thermal stratification and changing CH_4 production on hypolimnetic CH_4 dynamics, we developed a CH_4 model based on the hypolimnetic mass balance equation (Eq. 6; Supporting Information Fig. S2). The model predicts the hypolimnetic CH_4 concentration at a daily time step based on three parameters: effective diffusivity at the thermocline ($K_{z,\mathrm{eff}}$), gas transfer velocity across SWI (k_{sed}), and CH_4 production rate in sediments. First, we performed a model calibration by fitting parameter $K_{z,\mathrm{eff}}$ to observed $F_{\mathrm{diff,AOI}}$ and parameter k_{sed} to measured $F_{\mathrm{diff,SWI}}$ in Soppensee in both 2016 and 2017 (Supporting Information Table S1 and Section S2). From this calibration, the model was able to accurately reproduce the hypolimnetic CH_4 concentrations measurements (Supporting Information Fig. S8a,b). Then by modulating the CH_4 production

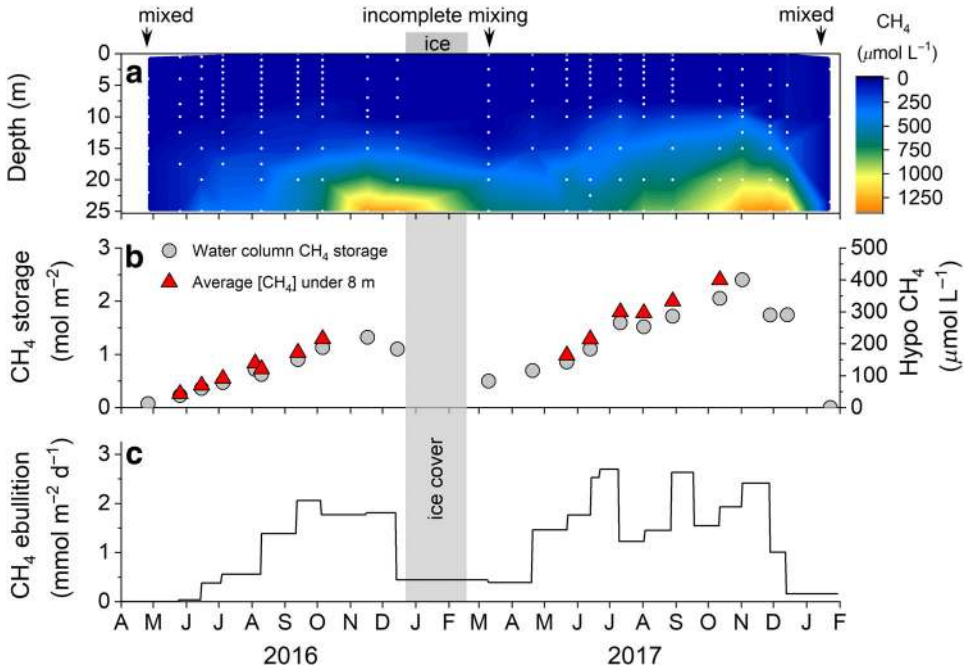

Fig. 4. Methane dynamics in Soppensee during 2016–2017. Panel (**a**) dissolved CH_4 contour plot measured at the deepest location and (**b**) whole water-column CH_4 storage (gray circles) and volume-weighted averaged CH_4 concentration below 8 m (red triangles) during the summer stratification periods. Panel (**c**) spatially averaged CH_4 ebullition below 8 m at SWI. White dots in panel (**a**) show the dissolved CH_4 sampling resolution.

within the observed range in Soppensee, the model was able to reproduce the ranges of the observed CH_4 ebullition rates (Supporting Information Fig. S8c,d). The model was then used to simulate a changing thermocline K_z under three different CH_4 production rates (Fig. 5). This modeling exercise revealed that storage rate (here represented as averaged hypolimnetic CH_4 concentration) is strongly affected by the reduced diffusive flux across the AOI associated with a decreasing K_z value. That is, as K_z becomes smaller, the proportion of CH_4 production going into storage increases, whereas the proportion going out to the upper layers decreases. The CH_4 ebullitive flux is primarily driven by CH_4 production rates, however, ebullitive rates are secondarily affected by the accumulation of methane in the hypolimnion (Langenegger et al. 2019) and therefore by K_z.

Table 1. Mass balance results comparing hypolimnetic (below 8 m) summer CH_4 dynamics (mmol m^{-2} d^{-1}) between late-April and early-October of 2016 and 2017. Values in brackets are the fluxes proportions of the CH_4 production (%). Uncertainties (± SD) for production and diffusion were determined from rules of error propagation (*see* Methods). Otherwise, uncertainty (±) represent the SD of the measurements.

		2016	2017
Net CH_4 production in sediment	P_{sed}	11.4 ± 1.3	17.7 ± 2.6
Fluxes at SWI			
Ebullitive flux	F_{ebu}	0.9 (8%)	1.9 (11%)
Diffusive flux	$F_{sed,diff}$	10.4 ± 1.2 (92%)	15.8 ± 2.5 (89%)
Fluxes at AOI			
Ebullitive flux	$(1-\alpha)F_{ebu}$	0.6 (6%)	1.3 (7%)
Diffusive flux	$F_{AOI,diff}$	1.6 ± 0.9 (13%)	4.7 ± 1.8 (27%)
Areal storage rate	$\frac{\Delta CH_4}{\Delta t}\frac{V_{hypo}}{A_{AOI}}$	9.2 ± 0.6 (81%)	11.7 ± 1.4 (66%)

Methane budget during mixing

We used a whole water-column mass balance to estimate the proportion of the stored CH_4 that was emitted during the fall/winter periods. During the first-year turnover including the ice-covered period (November 2016 to March 2017), averaged CH_4 surface diffusive fluxes were 0.7 mmol m^{-2} d^{-1} (Supporting Information Fig. S9a). During the second-year turnover (without ice, from November 2017 to January 2018) averaged CH_4 fluxes were 18 times higher at 12.7 mmol m^{-2} d^{-1} (Supporting Information Fig. S9b). In 2016, we observed the whole water-column CH_4 storage decrease linearly at a rate of 7.2 mmol m^{-2} d^{-1} between 17 November 2016 and 10 March 2017. In 2017, whole water-column CH_4 storage also decreased linearly at a rate of 28.9 mmol of CH_4 m^{-2} d^{-1} between 02 November 2017 and 23 January 2018. As a result, about 10% and 44% of whole water-column storage net loss rate was due to atmospheric diffusive emission in 2016 and 2017, respectively.

Discussion

Assessing sediment CH_4 rates from mass balances

By using a mass balance approach, we were able to estimate CH_4 diffusive fluxes and net production rates from hypolimnetic sediments during the summer stratified seasons of two

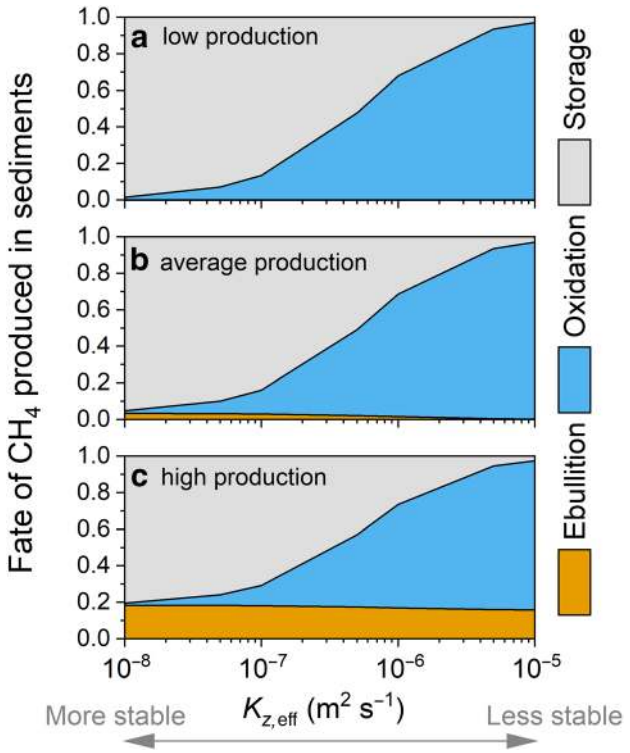

Fig. 5. Role of turbulent vertical diffusivity at the thermocline ($K_{z,eff}$) on the fate of CH_4 produced in the hypolimnetic sediments after 250 d of simulation. The different panels show CH_4 production rates in the sediments varying within the range estimated in Soppensee: (**a**) 10 mmol m^{-2} d^{-1} (low production), (**b**) 14 mmol m^{-2} d^{-1} (average production), and (**c**) 18 mmol m^{-2} d^{-1} (high production). For these simulations, we used the average k_{sed} of both year calibrations (0.003 m d^{-1}).

consecutive years. The mass balance results for both years were compared with sediment flux measurements and potential CH_4 production rates determined from sediment cores used in a companion study (Langenegger et al. 2019; Table 2). Potential CH_4 production rates were determined from laboratory incubation of sediments collected from cores taken in July 2016, while diffusive sediment CH_4 fluxes were determined in situ from several cores retrieved in 2016 and 2017 (*see* Supporting Information S3 for further details). Both core measurements and mass balance approaches resulted in similar ranges in CH_4 diffusion at the SWI and production rates (Table 2) even though their spatial and temporal integrations are different. Core-derived rates were variable among samples indicating some within-lake spatial variability. This spatial variability can be due, for example, to depth and sampled location, which both influence the environmental conditions (e.g., light, oxygen level, and temperature) and the local organic matter quantity and quality. As the mass balance approach integrates this spatial variability, a full method comparison requires the core-derived estimates to be extrapolated spatially over the full depth range (from 8 to 26 m).

Table 2. Comparing sediment CH_4 production (P_{sed}) and sediment diffusion rates ($F_{sed,diff}$) derived from the mass balance and from field and laboratory measurements. All core measurements are detailed and reported in Langenegger et al. (2019). All rates are in mmol CH_4 m^{-2} d^{-1}. Modeled and measured rates are presented as average ± standard deviation.

			Measured	
		Mass balance	8–15 m (*n*)	21–26 m (*n*)
CH_4 production	P_{sed}			
2016		11.4 ± 1.2	11.2 ± 6.7 (3)	
2017		17.7 ± 2.6	—	
CH_4 diffusion	$F_{sed,diff}$			
2016		10.4 ± 1.1	8.7 (1)	9.5 ± 2.9 (2)
2017		15.8 ± 2.5	9.3 ± 2.1 (3)	21.3 ± 13.3 (3)

The accuracy of the CH_4 diffusion at the SWI and net production rates derived from mass balance depends on the different flux component uncertainties, which in our case is ebullition. Methane ebullition in lakes is highly variable in space and time and is thus probably the most uncertain flux. Achieving unbiased CH_4 ebullition estimates over a whole lake requires an extensive number of measurements at multiple locations (Wik et al. 2016). In our case, the extrapolation of two to three bubble traps estimates over the whole hypolimnetic area can be precarious, even if the lake is relatively small. Our different bubble traps show different ebullition rates among sites, the highest rates recorded by the 10-m funnel and the 15-m funnel the lowest. The temporal evolution of ebullition fluxes was (however) consistent among the different traps (Supporting Information Fig. S7), suggesting that most of the uncertainty is related to the spatial variability. It has been suggested that for two to three sampling locations, the risk of misestimating ebullition fluxes is between 25% and 50%, with a higher risk of underestimating (Wik et al. 2016). To evaluate the impact of underestimation on the mass balance rates, we performed a sensitivity analysis. Increasing ebullition by 50% resulted in a CH_4 production increase of 4% and 5% for 2016 and 2017, respectively. Increasing ebullition by 100% resulted in increasing CH_4 production by 8% and 11% for 2016 and 2017, respectively. Although ebullition is an important pathway for surface CH_4 emissions (Bastviken et al. 2004*a*), the ebullition fluxes at SWI of deep sediments have a relatively small impact on the estimates of CH_4 production from mass balance calculations. The current uncertainties around mass-balance–derived CH_4 production rates (11% and 15% for 2016 and 2017, respectively; Table 1) are mainly due to storage accumulation rates and diffusive flux at the AOI.

Additional uncertainties regarding estimates of CH_4 production and diffusion at the SWI may occur due to the unaccounted potential CH_4 oxidation occurring below 8 m. Here, we assumed no CH_4 oxidation due to the mostly anoxic conditions found below 8 m in Soppensee. However, CH_4 oxidation could still occur by microaerobic CH_4 oxidizing bacteria just below the AOI (Blees et al. 2014), by anaerobic CH_4 oxidizing bacteria at the surface of sediments (Schubert et al. 2011)

or in the anoxic bottom waters (Eller et al. 2005). We suspect that microaerobic CH_4 oxidation may have occurred just below the AOI as we observed relatively higher values of δ^{13}C-CH_4 just below 8 m (Fig. 3a,b). As CH_4 oxidation seemed to have occurred only between 8 and 10 m and mostly early in the season, we can assume a limited effect on the CH_4 budget. However, it is important to interpret the reported production rates and diffusion at the SWI here as net (i.e., gross rate minus potential oxidation), even though the reported rates derived by the mass balance compared well with the measurements (Table 2).

Summer stratification strength and fate of sediment-produced CH_4

Net hypolimnetic sediments CH_4 production and diffusive fluxes in Soppensee were comparable to fluxes estimated from a similar approach in two temperate oligotrophic lakes (Peter and Paul Lakes; Bastviken et al. 2008). Despite similar rates, the fate of the sediment-derived CH_4 was different. In Peter and Paul Lakes, the majority of the CH_4 produced in the deep layers was oxidized (67–80%), whereas in Soppensee, the majority was stored in the hypolimnion (66–81%; Table 1). We suggest that the low K_z values found in Soppensee may have prevented upward CH_4 diffusion at the AOI toward the oxygenated waters where it is oxidized, in line with our hypothesis that strong summer stratification should result in greater CH_4 storage and less oxidation at the thermocline (Fig. 1). K_z values between 6 and 10 m in Soppensee were comparable between both years, yet we observed different rates (and proportion) of storage and diffusive fluxes at the AOI (Table 1). In summer 2016, a greater proportion of the produced CH_4 was stored, while in 2017, CH_4 transport across the thermocline became relatively more important (Table 1). Although the average vertical diffusivities (K_z) at 6–10 m were comparable in both years (Supporting Information Figs. S4, S5), the CH_4 gradient approaching the AOI was much steeper in 2017 due to the upward migration of the methane front (Fig. 3). This was probably the result of the higher net CH_4 production in 2017 and higher starting concentrations, combined with the higher turbulent diffusivities K_z below the AOI (between 11 and 15 m; Supporting Information Fig. S5). Higher K_z below the AOI may have caused a more efficient vertical redistribution of CH_4 in the hypolimnion (Fig. 3c) and thus increased the gradient at the AOI and the CH_4 fluxes across the AOI. The potential reasons for the increase of the K_z in the layer from 11 to 15 m are to be further investigated and might be related to difference in energy inputs (i.e., wind forcing); however, these results highlight the importance of K_z at and below the AOI for the vertical CH_4 diffusion.

As measured K_z at AOI were similar in both years, we could not explicitly test the effect of K_z on CH_4 storage and vertical diffusion at the AOI, therefore we applied a system analytical approach (Fig. 5; Supporting Information Fig. S2). As expected, increasing $K_{z,eff}$ resulted in more CH_4 diffusion across the AOI and less storage in the hypolimnion. When CH_4 is diffused up to the oxic waters, it can be assumed that most of it will be oxidized. This assumption is based on the persistence of a CH_4 minimum between 6 and 8 m during the summer stratified period associated with higher δ^{13}C-CH_4 values (Fig. 3a,c). Alternatively, when stratification is strong and K_z values are low, more CH_4 will be protected from oxidation and thus be stored due to the reduced flux at the AOI (Fig. 5).

When CH_4 leaves via ebullition (instead of diffusion across the SWI), less CH_4 is stored in the hypolimnion and diffused across the AOI and more can directly reach the atmosphere (Schmid et al. 2017). In Soppensee, the proportion of CH_4 production leaving via ebullition was higher in 2017 than in 2016 (Table 1) and is likely partly caused by the CH_4 concentration accumulation in the bottom waters (Boehrer et al. 2017; Horn et al. 2017). Accumulated CH_4 in the water column effectively reduces the CH_4 gradient between porewater and overlaying water, thus diminishing the diffusive flux at the SWI (Langenegger et al. 2019). Assuming that $F_{ebu} = P_{sed} - F_{diff,SWI}$, reducing diffusive fluxes should have the effect of reallocating the produced CH_4 into ebullition. The model also confirmed that increasing storage by decreasing $K_{z,eff}$ slightly increases the proportion of CH_4 leaving by ebullition (Fig. 5c), an effect that is independent of sediment CH_4 production (i.e., similar decrease Fig. 5b,c). Looking at absolute rates of ebullition however, the effect of $K_{z,eff}$ is more apparent. For example, decreasing $K_{z,eff}$ from 10^{-6} to 10^{-7} m^2 s^{-1} will double the average ebullition rate (from about 0.5 to 1 mmol CH_4 m^{-2} d^{-1}) at CH_4 production ranges of 14–15 mmol m^{-2} d^{-1}. However, the same $K_{z,eff}$ reduction over a CH_4 production range of 17–18 mmol m^{-2} d^{-1} would cause ebullition rates to increase by about 10% (from about 3.5 to 3.9 mmol CH_4 m^{-2} d^{-1}).

Potential consequences of incomplete winter mixing on summer CH_4 dynamics

In 2017, net CH_4 production in the hypolimnion increased by nearly 60% compared to 2016. Although several factors may influence across-system differences in lake sediments CH_4 production (West et al. 2012, 2015), our results suggest the potential implications of incomplete mixing of the water column during the previous winter. In March 2016, dissolved O_2 penetrated deeper in the water column compared to March 2017, when anoxia persisted in the hypolimnetic waters (Supporting Information Fig. S10). We suggest that this persistence of anoxia in 2017 probably allowed better conditions for methanogenesis, as opposed to 2016, where anoxia gradually developed later in the season. As the stratification season progresses, the more energetically favorable electron acceptors (e.g., NO_3^-, Mn [IV], SO_4^{2-}) are no longer available for microbial anaerobic organic matter degradation, thus CH_4 production will likely dominate the overall biogeochemical transformations. For example, in March 2016, NO_3^- and SO_4^{2-} mean concentrations below 10 m were 325 μg L^{-1} and 6.6 mg L^{-1}, respectively, while in November 2016, both solutes were below detection limit below

10 m (Canton of Lucerne monitoring program). As the lake did not mix completely in winter 2016/2017, these solutes remained depleted, or at least very low, in the bottom waters in spring 2017. Complete fall/winter turnover is thus an important "reset" for the redox balance (Lehmann et al. 2015). This phenomenon was also reported in a tropical reservoir (Itoh et al. 2015) and strengthens our interpretation that with meromixis/incomplete mixing, the lake system becomes more efficient at producing CH_4 for a given supply of organic material (e.g., from primary production).

Methane ebullition might also have been influenced by the incomplete mixing. Although a lot of factors may contribute, including oxidation pathways, temperature, and supplies of organic material, ebullition did not begin until about June 2016 when bottom water concentrations of CH_4 began to build up significantly (Fig. 4). The ebullition rate continued to increase during the season as hypolimnetic CH_4 continued to increase (Fig. 4b,c). This link between CH_4 ebullition and bottom concentration was also noticeable in winter. Low but active CH_4 ebullition was measured during winter 2016/2017 as the CH_4 concentration, though reduced, remained at relatively high levels due to the incomplete turnover. In winter 2017/2018, CH_4 ebullition ceased with complete lake turnover and CH_4 was almost completely removed from the water column. However, while this process alone does not a priori change the overall CH_4 flux from sediment (i.e., production, see the following discussion on potential effect on production), it could potentially increase the amount of CH_4 reaching the atmosphere, as CH_4 leaving via ebullition is more likely to escape oxidation.

Fate of CH_4 storage during fall vertical mixing

As an important amount of CH_4 is stored in the hypolimnion in stratified lakes, the fate of this CH_4 when the lake does turnover in fall/winter is critical for annual CH_4 emission budgets. Our results show the marked difference in CH_4 dynamics during the turnover period of both years, where the net CH_4 loss rate (CH_4 storage decrease rate; Fig. 4b) in 2017 was significantly greater than in 2016. This suggests that both CH_4 oxidation and evasion to the atmosphere were more important during fall 2017 compared to fall 2016, where a portion of the stored CH_4 remained in the bottom waters over winter. By estimating the diffusive CH_4 fluxes to the atmosphere during these periods, we found that a higher proportion was emitted the second year (44%) compared to the first year (10%). However, these estimates rely on the CH_4 emissions estimates, which in our case were constrained by the low temporal resolution of the sampling. We compared the flux derived from the wind-speed model with floating chambers measurements. Although they are comparable most of the time, the floating chamber CH_4 flux estimates showed much higher values in December 2017 compared to the modeled flux used in this calculation (Supporting Information Fig. S9b). Thus, using the generally lower wind-model–derived estimate, we consider our estimates to be conservative. Determining with precision the proportion emitted vs. oxidized however requires high temporal resolution CH_4 flux or oxidation rate measurements (Schubert et al. 2012; Encinas Fernández et al. 2014).

The estimate of the proportion of stored CH_4 that is emitted during fall was completely different between years (10% and 44%). In 2016–2017, the winter was colder, and the lake was quickly ice-covered in early January to end of February 2017. Consequently, the mixing was incomplete (down to 19 m instead of the maximum depth of 26 m) and lasted about 120 d until the upper mixed layer reached about 19 m. Conversely, the winter of 2017–2018 was warmer with strong wind events (Supporting Information Fig. S9) and no ice formation, resulting in complete turnover (down to the bottom) in 82 d. The turnover was so rapid in fact that the lake became completely anoxic, even in the surface waters, for about 10 d (Fig. 2d). We suggest that the potentially higher proportion of CH_4 emitted in 2017–2018 was due to a combination of the lower O_2 content in the water column, the complete anoxia episode (thus negligible CH_4 oxidation), and the more efficient vertical mixing. We compared the results from Soppensee to published values and found a linear relationship between the speed of mixing (lake maximum depth divided by mixing duration) and the proportion of CH_4 emitted during that period (Fig. 6). Although nonsignificant, this relationship suggests that a rapid and constant mixing will favor higher CH_4 emissions. If the lake mixes slowly, with occasional restratification and/or ice formation, a

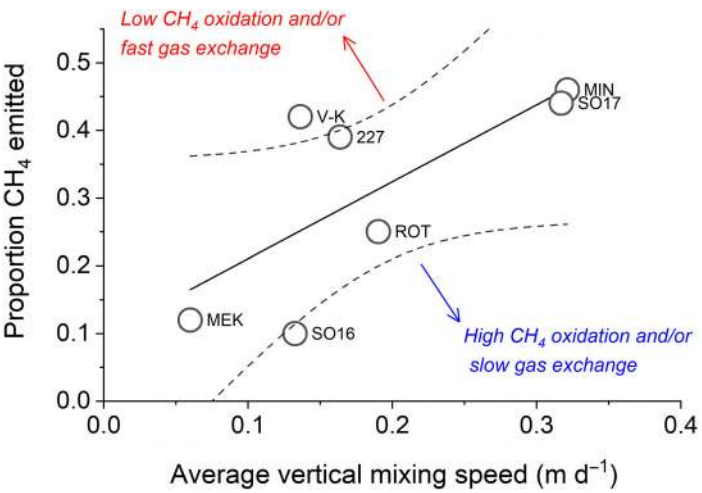

Fig. 6. Relationship between the average vertical mixing speed (m d^{-1}) and proportion of stored CH_4 that was emitted during fall/winter mixing ($R^2 = 0.52$, $p = 0.07$). SO16 and SO17 are from this study, ROT is Lake Rotsee (Schubert et al. 2012), MIN is Lake Minglesee (Encinas Fernández et al. 2014), 227 is Lake 227 (Rudd and Hamilton 1978), MEK is Lake Mekkojarvi (Kankaala et al. 2007), and V-K is lake Valkea-Kotinen (Kankaala et al. 2006). Published estimates of proportions emitted were calculated with a mass balance during fall turnover period, except for V-K, where the proportion emitted value was calculated as the amount of CH_4 emitted divided by the total loss during fall turnover (emissions + oxidation). Solid line is the linear regression fit with 95% confident interval (dashed lines).

higher proportion of the stored CH_4 will be oxidized (Kankaala et al. 2007). The lakes departure from the regression line (red and blue arrows) suggest that some lakes are more or less efficient to oxidize CH_4 (e.g., due to biological or chemical reasons) and some lakes are more or less efficient to exchange gas (e.g., due to morpho-physical reasons; Vachon and Prairie 2013).

High CH_4 oxidation rates suggest that the lake O_2 can be highly stressed during fall/winter turnover, as 1 mol of CH_4 consume 2 mol of O_2 during oxidation. Using this stoichiometric conversion, in early November 2016, the CH_4 content in the whole lake would have been enough to consume 1.2 times the whole-lake O_2 content (assuming instantaneous mixing and no supply of O_2). In November 2017, the CH_4 content alone could have consumed 2.4 times the O_2 content. The combination of incomplete mixing in winter 2016–2017 and higher CH_4 production during the following summer led to extreme CH_4 storage in 2017. This high CH_4 content (in addition to the accumulation of other reduced solutes, e.g., NH_4, HS^-, Mn(II), and Fe(II)) put an enormous stress on the lake O_2 content (Müller et al. 2012), and as the lake completely mixed during winter 2017–2018, the O_2 atmospheric inputs were not enough to avoid complete anoxia (Fig. 2d). By affecting O_2, episodes of incomplete followed by complete mixing can have crucial consequences on the whole-lake ecology in addition to the lake CH_4 dynamics.

Conclusions

Here, we showed that, independent of biological CH_4 production and oxidation processes, the physical environment of lakes greatly regulates the fate of CH_4 produced in the deeper sediments of stratified systems. Environmental-driven physical changes to the lake seasonal hydrodynamics—e.g., induced by climate change, eutrophication, or browning—will certainly impact lakes CH_4 dynamics, emissions and the overall carbon flow in the system. For example, warmer summers will potentially lead to longer stratified seasons and stronger density gradients (Winslow et al. 2014; Butcher et al. 2015). Similarly, browning or decreased water transparency due to biomass growth (eutrophication) could also result in stronger density gradients (Foley et al. 2012). Our results suggest that these environmental changes affecting lake physics could potentially increase the role of CH_4 production, CH_4 storage, and ebullition from lakes during the summer months and concurrently reduce CH_4 oxidation at the thermocline. Such a scenario of strong summer stratification (resulting in higher K_z; Fig. 5) combined with rapid water mixing in fall/winter (Fig. 6) could potentially increase the proportion of stored CH_4 in the lake bottom waters to be emitted to the atmosphere instead of being oxidized. The exact response of lake CH_4 dynamics to changes in lake hydrodynamics is however very challenging to predict, as these potential environmental and climate changes also affect biological processes, with possibilities for complex interactions and positive feedbacks. Disentangling the respective roles of physics and biology in regulating CH_4 in lakes however greatly improves our current understanding and provides better tools to assess the system-specific sensitivity of such environmental and climate changes.

References

Adams, D. D. 2005. Diffuse flux of greenhouse gases—methane and carbon dioxide—at the sediment-water Interface of some lakes and reservoirs of the world, p. 129–153. *In* A. Tremblay, L. Varfalvy, C. Roehm, and M. Garneau [eds.], Greenhouse gas emissions—fluxes and processes: Hydroelectric reservoirs and natural environments. Springer. doi:10.1007/978-3-540-26643-3_6

Bastviken, D., J. Cole, M. Pace, and L. Tranvik. 2004*a*. Methane emissions from lakes: Dependence of lake characteristics, two regional assessments, and a global estimate. Global Biogeochem. Cycles **18**: 1–12. doi:10.1029/2004GB002238

Bastviken, D., L. Persson, G. Odham, and L. Tranvik. 2004*b*. Degradation of dissolved organic matter in oxic and anoxic lake water. Limnol. Oceanogr. **49**: 109–116. doi:10.4319/lo.2004.49.1.0109

Bastviken, D., J. J. Cole, M. L. Pace, and M. C. Van de Bogert. 2008. Fates of methane from different lake habitats: Connecting whole-lake budgets and CH_4 emissions. J. Geophys. Res. Biogeo. **113**: 1–13. doi:10.1029/2007JG000608

Bastviken, D., L. J. Tranvik, J. A. Downing, P. M. Crill, and A. Enrich-Prast. 2011. Freshwater methane emissions offset the continental carbon sink. Science **331**: 6. doi:10.1126/science.1196808

Blees, J., and others. 2014. Micro-aerobic bacterial methane oxidation in the chemocline and anoxic water column of deep south-alpine Lake Lugano (Switzerland). Limnol. Oceanography **59**: 311–324. doi:10.4319/lo.2014.59.2.0311

Boehrer, B., C. von Rohden, and M. Schultze. 2017. Physical features of Meromictic Lakes: Stratification and circulation. *In* R. D. Gulati, S. Zadereev, Egor, and A. G. Degermendzhy [eds.], Ecology of Meromictic Lakes. Springer.

Bogard, M. J., P. A. del Giorgio, L. Boutet, M. C. G. Chaves, Y. T. Prairie, A. Merante, and A. M. Derry. 2014. Oxic water column methanogenesis as a major component of aquatic CH_4 fluxes. Nat. Commun. **5**: 5350. doi:10.1038/ncomms6350

Butcher, J. B., D. Nover, T. E. Johnson, and C. M. Clark. 2015. Sensitivity of lake thermal and mixing dynamics to climate change. Clim. Change **129**: 295–305. doi:10.1007/s10584-015-1326-1

Carey, C. C., R. P. McClure, J. P. Doubek, M. E. Lofton, N. K. Ward, and D. T. Scott. 2018. *Chaoborus* spp. transport CH_4 from the sediments to the surface waters of a eutrophic reservoir, but their contribution to water column CH_4 concentrations and diffusive efflux is minor. Environ. Sci. Technol. **52**: 1165–1173. doi:10.1021/acs.est.7b04384

Carmichael, M. J., E. S. Bernhardt, S. L. Bräuer, and W. K. Smith. 2014. The role of vegetation in methane flux to the atmosphere: Should vegetation be included as a distinct

category in the global methane budget? Biogeochemistry **119**: 1–24. doi:10.1007/s10533-014-9974-1

Chanton, J. P., C. S. Martens, and C. A. Kelley. 1989. Gas transport from methane-saturated, tidal freshwater and wetland sediments. Limnol. Oceanogr. **34**: 807–819. doi:10.4319/lo.1989.34.5.0807

Crusius, J., and R. Wanninkhof. 2003. Gas transfer velocities measured at low wind speed over a lake. Limnol. Oceanogr. **48**: 1010–1017. doi:10.4319/lo.2003.48.3.1010

DelSontro, T., D. F. McGinnis, S. Sobek, I. Ostrovsky, and B. Wehrli. 2010. Extreme methane emissions from a Swiss hydropower reservoir: Contribution from bubbling sediments. Environ. Sci. Technol. **44**: 2419–2425. doi:10.1021/es9031369

Donis, D., S. Flury, A. Stöckli, J. E. Spangenberg, D. Vachon, and D. F. McGinnis. 2017. Full-scale evaluation of methane production under oxic conditions in a mesotrophic lake. Nat. Commun. **8**: 1661. doi:10.1038/s41467-017-01648-4

Eller, G., L. Känel, and M. Krüger. 2005. Cooccurrence of aerobic and anaerobic methane oxidation in the water column of Lake Plußsee. Appl. Environ. Microbiol. **71**: 8925–8928. doi:10.1128/AEM.71.12.8925

Encinas Fernández, J., F. Peeters, and H. Hofmann. 2014. Importance of the autumn overturn and anoxic conditions in the hypolimnion for the annual methane emissions from a temperate lake. Environ. Sci. Technol. **48**: 7297–7304. doi:10.1021/es4056164

Fallon, R. D., S. Harrits, R. S. Hanson, and T. D. Brock. 1980. The role of methane in internal carbon cycling in Lake Mendota during summer stratification. Limnol. Oceanogr. **25**: 357–360. doi:10.4319/lo.1980.25.2.0357

Foley, B., I. D. Jones, S. C. Maberly, and B. Rippey. 2012. Long-term changes in oxygen depletion in a small temperate lake: Effects of climate change and eutrophication. Freshw. Biol. **57**: 278–289. doi:10.1111/j.1365-2427.2011.02662.x

Grasset, C., R. Mendonça, G. Villamor Saucedo, D. Bastviken, F. Roland, and S. Sobek. 2018. Large but variable methane production in anoxic freshwater sediment upon addition of allochthonous and autochthonous organic matter. Limnol. Oceanogr. **63**: 1488–1501. doi:10.1002/lno.10786

Horn, C., P. Metzler, K. Ullrich, M. Koschorreck, and B. Boehrer. 2017. Methane storage and ebullition in monimolimnetic waters of polluted mine pit lake Vollert-Sued, Germany. Sci. Total Environ. **584–585**: 1–10. doi:10.1016/j.scitotenv.2017.01.151

Imboden, D. M., and A. Wüest. 1995. Mixing mechanisms in lakes, p. 83–138. *In* A. Lerman, A. Wüest, and J. R. Gat [eds.], Physics and chemistry of lakes. Springer-Verlag.

Itoh, M., and others. 2015. Effect of interannual variation in winter vertical mixing on CH_4 dynamics in a subtropical reservoir. J. Geophys. Res. Biogeosci. **120**: 1246–1261. doi:10.1002/2015JG002972

Jähne, B., K. O. Münnich, R. Bösinger, A. Dutzi, W. Huber, and P. Libner. 1987. On the parameters influencing air-water gas exchange. J. Geophys. Res. Oceans **92**: 1937–1949. doi:10.1029/JC092iC02p01937

Jassby, A., and T. Powell. 1975. Vertical patterns of eddy diffusion during stratification in Castle Lake, California. Limnol. Oceanogr. **20**: 530–543. doi:10.4319/lo.1975.20.4.0530

Juutinen, S. 2003. Major implication of the littoral zone for methane release from boreal lakes. Global Biogeochem. Cycles **17**: 1–11. doi:10.1029/2003GB002105

Juutinen, S., M. Rantakari, P. Kortelainen, J. T. Huttunen, T. Larmola, J. Alm, J. Silvola, and P. J. Martikainen. 2009. Methane dynamics in different boreal lake types. Biogeosciences **6**: 209–223. doi:10.5194/bg-6-209-2009

Kankaala, P., J. Huotari, E. Peltomaa, T. Saloranta, and A. Ojala. 2006. Methanotrophic activity in relation to methane efflux and total heterotrophic bacterial production in a stratified, humic, boreal lake. Limnol. Oceanogr. **51**: 1195–1204. doi:10.4319/lo.2006.51.2.1195

Kankaala, P., S. Taipale, H. Nykänen, and R. I. Jones. 2007. Oxidation, efflux, and isotopic fractionation of methane during autumnal turnover in a polyhumic, boreal lake. J. Geophys. Res. Biogeosci. **112**: 1–7. doi:10.1029/2006JG000336

Kankaala, P., J. Huotari, T. Tulonen, and A. Ojala. 2013. Lake-size dependent physical forcing of carbon dioxide and methane effluxes from lakes in a boreal landscape. Limnol. Oceanogr. **58**: 1915–1930. doi:10.4319/lo.2013.58.6.1915

Kirschke, S., and others. 2013. Three decades of global methane sources and sinks. Nat. Geosci. **6**: 813–823. doi:10.1038/ngeo1955

Kreling, J., J. Bravidor, D. F. McGinnis, M. Koschorreck, and A. Lorke. 2014. Physical controls of oxygen fluxes at pelagic and benthic oxyclines in a lake. Limnol. Oceanogr. **59**: 1637–1650. doi:10.4319/lo.2014.59.5.1637

Langenegger, T., D. Vachon, D. Donis, and D. F. McGinnis. 2019. What the bubble knows: Lake methane dynamics revealed by sediment gas bubble composition. Limnol. Oceanogr. doi:10.1002/lno.11133

Lehmann, M. F., M. Simona, S. Wyss, J. Blees, C. H. Frame, H. Niemann, M. Veronesi, and J. Zopfi. 2015. Powering up the "biogeochemical engine": the impact of exceptional ventilation of a deep meromictic lake on the lacustrine redox, nutrient, and methane balances. Front. Earth Sci. **3**: 45. doi:10.3389/feart.2015.00045

MacIntyre, S., A. Jonsson, M. Jansson, J. Aberg, D. E. Turney, and S. D. Miller. 2010. Buoyancy flux, turbulence, and the gas transfer coefficient in a stratified lake. Geophys. Res. Lett. **37**: L24604. doi:10.1029/2010GL044164

McGinnis, D. F., J. Greinert, Y. Artemov, S. E. Beaubien, and A. Wüest. 2006. Fate of rising methane bubbles in stratified waters: How much methane reaches the atmosphere? J. Geophys. Res. **111**: C09007. doi:10.1029/2005JC003183

McGinnis, D. F., G. Kirillin, K. W. Tang, S. Flury, P. Bodmer, C. Engelhardt, P. Casper, and H.-P. Grossart. 2015. Enhancing surface methane fluxes from an oligotrophic Lake: Exploring

the microbubble hypothesis. Environ. Sci. Technol. **49**: 873–880. doi:10.1021/es503385d

McGinnis, D. F., S. Flury, K. W. Tang, and H.-P. Grossart. 2017. Porewater methane transport within the gas vesicles of diurnally migrating *Chaoborus* spp.: An energetic advantage. Sci. Rep. **7**: 44478. doi:10.1038/srep44478

Müller, B., L. D. Bryant, A. Matzinger, and A. Wüest. 2012. Hypolimnetic oxygen depletion in eutrophic lakes. Environ. Sci. Technol. **46**: 9964–9971. doi:10.1021/es301422r

Oswald, K., J. Milucka, A. Brand, P. Hach, S. Littmann, B. Wehrli, M. M. M. Kuypers, and C. J. Schubert. 2016. Aerobic gammaproteobacterial methanotrophs mitigate methane emissions from oxic and anoxic lake waters. Limnol. Oceanogr. **61**: S101–S118. doi:10.1002/lno.10312

Read, J. S., and others. 2012. Lake-size dependency of wind shear and convection as controls on gas exchange. Geophys. Res. Lett. **39**: 39. doi:10.1029/2012GL051886

Reed, D. C., B. R. Deemer, S. van Grinsven, and J. A. Harrison. 2017. Are elusive anaerobic pathways key methane sinks in eutrophic lakes and reservoirs? Biogeochemistry **134**: 29–39. doi:10.1007/s10533-017-0356-3

Rinta, P., D. Bastviken, J. Schilder, M. Van Hardenbroek, T. Stötter, and O. Heiri. 2017. Higher late summer methane emission from central than northern European lakes. J. Limnol. **76**: 52–67. doi:10.4081/jlimnol.2016.1475

Rudd, J. W. M., and R. D. Hamilton. 1978. Methane cycling in a eutrophic shield lake and its effects on whole lake metabolism. Limnol. Oceanogr. **23**: 337–348. doi:10.4319/lo.1978.23.2.0337

Sander, R. 1999. Compilation of Henry's law constants for inorganic and organic species of potential importance in environmental chemistry. Database **20**: 107. doi:10.1017/CBO9781107415324.004

Schmid, M., I. Ostrovsky, and D. F. McGinnis. 2017. Role of gas ebullition in the methane budget of a deep subtropical lake: What can we learn from process-based modeling? Limnol. Oceanogr. **62**: 2674–2698. doi:10.1002/lno.10598

Schubert, C. J., T. Diem, and W. Eugster. 2012. Methane emissions from a small wind shielded lake determined by eddy covariance, flux chambers, anchored funnels, and boundary model calculations: A comparison. Environ. Sci. Technol. **46**: 4515–4522. doi:10.1021/es203465x

Schubert, C. J., F. Vazquez, T. Lösekann-Behrens, K. Knittel, M. Tonolla, and A. Boetius. 2011. Evidence for anaerobic oxidation of methane in sediments of a freshwater system (Lago di Cadagno). FEMS Microbiol. Ecol. **76**: 26–38. doi:10.1111/j.1574-6941.2010.01036.x

Schultze, M., B. Boehrer, K. Wendt-Potthoff, S. Katsev, and E. T. Brown. 2017. Chemical setting and biogeochemical reactions in Meromictic Lakes. *In* R. D. Gulati, E. S. Zadereev, and A. G. Degermendzhi [eds.], Ecology of Meromictic Lakes. Springer.

Sundh, I., D. Bastviken, and L. J. Tranvik. 2005. Abundance, activity, and community structure of pelagic methane-oxidizing bacteria in Temperate Lakes. Appl. Environ. Microbiol. **71**: 6746–6752. doi:10.1128/AEM.71.11.6746

Utsumi, M., Y. Nojiri, T. Nakamura, T. Nozawa, A. Otsuki, N. Takamura, M. Watanabe, and H. Seki. 1998. Dynamics of dissolved methane and methane oxidation in dimictic Lake Nojiri during winter. Limnol. Oceanogr. **43**: 10–17. doi:10.4319/lo.1998.43.1.0010

Vachon, D., and Y. T. Prairie. 2013. The ecosystem size and shape dependence of gas transfer velocity versus wind speed relationships in lakes. Can. J. Fish. Aquat. Sci. **70**: 1757–1764. doi:10.1139/cjfas-2013-0241

Wanninkhof, R. 1992. Relationship between wind speed and gas exchange over the ocean. J. Geophys. Res. Oceans **97**: 7373–7382. doi:10.1029/92JC00188

West, W. E., J. J. Coloso, and S. E. Jones. 2012. Effects of algal and terrestrial carbon on methane production rates and methanogen community structure in a temperate lake sediment. Freshw. Biol. **57**: 949–955. doi:10.1111/j.1365-2427.2012.02755.x

West, W. E., S. M. Mccarthy, and S. E. Jones. 2015. Phytoplankton lipid content influences freshwater lake methanogenesis. Freshw. Biol. **60**: 2261–2269. doi:10.1111/fwb.12652

West, W. E., K. P. Creamer, and S. E. Jones. 2016. Productivity and depth regulate lake contributions to atmospheric methane. Limnol. Oceanogr. **61**: S51–S61. doi:10.1002/lno.10247

Wik, M., B. F. Thornton, D. Bastviken, J. Uhlbäck, and P. M. Crill. 2016. Biased sampling of methane release from northern lakes: A problem for extrapolation. Geophys. Res. Lett. **43**: 1256–1262. doi:10.1002/2015GL066501

Winslow, L. A., J. S. Read, G. J. A. A. Hansen, and P. C. Hanson. 2014. Small lakes show muted climate change signal in deepwater temperatures. Geophys. Res. Lett. **42**: 355–361. doi:10.1002/2014GL062325

Wüest, A., G. Piepke, and D. C. Van Senden. 2000. Turbulent kinetic energy balance as a tool for estimating vertical diffusivity in wind-forced stratified waters. Limnol. Oceanogr. **45**: 1388–1400. doi:10.4319/lo.2000.45.6.1388

Acknowledgments

We would like to thank Sabine Flury and César Ordóñez for help in the field and the Canton of Lucerne for providing chemistry data. We thank Bernhard Pfyffer for providing access to the lake and infrastructure and Philippe Arpagaus for help with laboratory measurements. We also thank Rolf Kipfer and Matthias Brennwald for lending us their Picarro (Picarro G2201-i) system and two anonymous reviewers for their insightful comments. This study was funded by the Swiss National Science Foundation (SNSF grant 200021_160018, Bubble Flux).

Conflict of Interest

None declared.

Submitted 18 September 2018
Revised 01 February 2019
Accepted 14 March 2019

Associate editor: John Downing